ADVANCING EARTH AND SPACE SCIENCE

JGR Oceans

RESEARCH ARTICLE

10.1029/2021JC017964

Coastal Hazards of Tropical-Like Cyclones Over the Mediterranean Sea

Tim Toomey[1], Angel Amores[1], Marta Marcos[1,2], Alejandro Orfila[1], and Romualdo Romero[2]

[1]Mediterranean Institute for Advanced Studies (UIB-CSIC), Esporles, Spain, [2]Department of Physics, University of the Balearic Islands, Palma, Spain

Key Points:

- Mediterranean hurricanes (medicanes) generate largest wind-waves (exceeding 10 m) in the central and the southwest part of the western basin
- Wide and gently sloping continental shelves favor the generation of storm surges under medicane forcing with 100-year return levels over 1 m
- Projected changes medicane-induced coastal hazards are uncertain due to limited multimodel consensus, with some local exceptions

Correspondence to:

T. Toomey,
tim.toomey@uib.es

Citation:

Toomey, T., Amores, A., Marcos, M., Orfila, A., & Romero, R. (2022). Coastal hazards of tropical-like cyclones over the Mediterranean Sea. *Journal of Geophysical Research: Oceans*, *127*, e2021JC017964. https://doi.org/10.1029/2021JC017964

Received 1 SEP 2021
Accepted 2 FEB 2022

Abstract Medicanes, for Mediterranean hurricanes, are mesoscale cyclones with morphological and physical characteristics similar to tropical cyclones. Although less intense, smaller, and rarer than their Atlantic counterparts, medicanes are very hazardous events threatening islands and continental coasts within the Mediterranean Sea. The latest strong episode, Medicane Ianos (September 2020), resulted in severe damages in Greece and several casualties. This work investigates the oceanic response to these extreme events along the Mediterranean coasts under present-day and future (late 21st century) climate conditions. To this end, a coupled hydrodynamic-wave model is used to simulate both storm surges and wind-waves generation and propagation in the Mediterranean Sea at high resolution (~2 km) along the coastlines. A data set of thousands of medicanes synthetically generated from 20 global climate models and two atmospheric reanalyses is used to derive the atmospheric forcing fields. Regional coastal hazards assessment is performed for the present and future climates. For the first period, highest medicane-induced waves are found in the central and the southwest part of the western Mediterranean, while greatest storm surges are found in the Adriatic Sea and regions characterized by wide and gently sloping continental shelves. Results obtained for future changes show amplitudes generally smaller than the associated uncertainty due to limited agreement among models (especially for coastal elevation). Though, model consensus is reached (60–75%) and relative intensity change is significant (10–20%) at some locations (e.g., 1 m increase of medicane-induced significant wave height on average for south coasts of Sicilia).

Plain Language Summary Mediterranean hurricanes, medicanes, are tropical-like cyclones generated in the Mediterranean basin that differ from their counterpart in the Atlantic in their smaller size and intensity. They rarely exceed 400 km of diameter and last generally 24–48 hr, unusually reaching intensities of category 1 hurricanes. A medicane is characterized by a warm core accompanied by thunderstorms, heavy rain, but also strong cyclonic winds (counter-clockwise rotation) that are responsible for costly damages and often result in casualties. Furthermore, medicanes pose serious threats to coastal populations due to the storm surges, that is, the raising of the sea surface due to low atmospheric pressure, and to the combined effects of waves and winds along the coasts. This study investigates the coastal hazards induced by medicanes over the entire basin. To do so, we used a hydrodynamic and wave coupled model to simulate the generation and propagation of storm surges and wind-waves over the Mediterranean Sea under the forcing of a set of thousands of synthetic medicanes that statistically describe the medicane climate for the present and future period (end of 21st century). Our results identify the most exposed coastal areas and quantify the current and projected return levels for waves and storm surges.

1. Introduction

The Mediterranean Sea is a semienclosed basin and a region with very frequent cyclogenesis events. Its complex orography together with low-level baroclinicity and low-level moisture sources favor a wide range of cyclogenesis mechanisms (Campins et al., 2011; Jansà, 1997; Sartini et al., 2015; Trigo et al., 2002). Occasionally, tropical-like cyclones (called "medicanes," as contraction of Mediterranean hurricanes) develop and evolve over the Mediterranean with very similar characteristics to most known occurring in large ocean basins. Medicanes are characterized by a cyclonic axisymmetric structure, with cloud bands wrapped around a low-pressure and warm core at the center. Although showing generally smaller radius than hurricanes, medicanes sometimes reach similar strength in terms of wind intensity (up to category 1 events; Emanuel, 2005; Fita et al., 2007; Romero & Emanuel, 2013). Therefore, these storms pose serious threats on coastal populations, assets and activities located in the vicinity of

Table 1
Characteristics of Simulated Real Medicanes

Medicane	Querida	Rolf	Numa	Ianos
Spanning Period	September 26–27, 2006	November 6–10, 2011	November 12–19, 2017	September 14–20, 2020
Max. Wind speed (m/s)	18.9	19.6	22.3	18
Min. Prmsl (hPa)	997	1,002	990	1,000
Tide gauges N°	41	27	59	83
Wave buoys N°	18	24	25	23
Casulaties, cost	–, –	12 fatalities, US$1.25 billion (*)	21 fatalities in Greece, US$100 million (°)	Four fatalities (+), –

Note. Maximum wind speed and minimum pressure at mean sea level (Prmsl) are extracted From ERA5 data set. "–" Means Undocumented. Sources are: http://thoughtleadership.aon.com/documents/201112_if_monthly_cat_recap_november.pdf; https://www.eumetsat.int/tropical-storm-develops-mediterranean-sea for (*); http://thoughtleadership.aon.com/Documents/20171207-ab-analytics-if-november-global-recap.pdf; https://www.aljazeera.com/news/2017/11/19/storm-numa-forms-in-the-mediterranean/; https://www.bloomberg.com/news/articles/2017-11-21/storm-that-unleashed-deadly-floods-in-greece-was-rare-medicane for (°); https://www.euronews.com/2020/09/17/cyclone-ianos-greek-authorities-issue-warning-for-rare-extreme-weather-phenomenon;https://www.bbc.com/news/world-europe-54219180 for (+).

their tracks (Bakkensen, 2017), because of their intense winds, precipitation and coastal flooding due to storm surges and wind-waves hitting coasts (see Table 1 for historical medicane-induced damages).

Unlike their neighbors in the Atlantic, medicanes are relatively rare phenomena. As it is difficult to formulate a clear distinction between medicanes and the broad spectrum of Mediterranean low-pressure systems, the use of criteria more or less strict can induce varying results on the average occurrence of these storms, for example, 0.5 (Tous & Romero, 2013), 1.6 (Cavicchia et al., 2013), or 2 events/year (Romero & Emanuel, 2016). Nonetheless, all previous studies agree on the fact that medicanes occur with low frequency in time. In addition of their rarity, these phenomena occur over spatially limited regions. Therefore, length of simulation (e.g., hindcasts) or availability of in situ data over limited time and spatial range are insufficient to estimate return periods of extreme events (whether for atmospheric or ocean components). One way to overcome this issue is to take advantage of synthetically generated events from statistical methods based on historical data or projected simulations. Based on previous works, Romero and Emanuel (2016) adapted the original method (Emanuel, 2006) for warm-cored tropical cyclones to the more specific midlatitude synoptic development of medicanes (Romero & Emanuel, 2013), originating from deep, cut-off, cold-core lows in the uppertroposphere and midtroposphere. The authors characterized the medicane climate for the present and future periods through a statistic-deterministic approach that generates thousands of synthetics medicanes tracks from atmospheric fields, performing wind risk assessments for both periods at Mediterranean scale. Apart from extreme winds and precipitation, medicane interaction with the sea surface generates and propagates hazardous waves and storm surges that also are likely to cause damages along Mediterranean coasts.

Complementary to the Romero and Emanuel (2016) study, but with an approach focusing on marine effects, the aim of this work is to quantify the coastal impacts caused by the so-called medicanes along the Mediterranean coastline in present-day climate and under projected climate change scenarios for the late 21st century. To do so, we have dynamically modeled the storm surges and wind-waves generated by atmospheric fields during the occurrence of medicanes within the Mediterranean basin. The outputs were used to investigate their potential impacts along the coasts. The manuscript is organized as follows: Section 2 resumes the data and methods used: the numerical model and its configuration are described, along with atmospheric fields and in situ data used for the validation of modeled storm surges and waves. Moreover, the description of the original present-day and future climate data set of synthetic medicanes from Romero and Emanuel (2016) is provided. Simulating real medicanes, modeled outputs over the ocean are compared with in situ sea level and wave observations in Section 3. The description of the synthetic medicanes selected and simulated along with the method used to analyze the outputs is provided in Section 4. Medicane-induced perturbations of ocean components (coastal sea surface elevation and significant wave height) are analyzed at Mediterranean scale for the present and future climate in Section 5. Finally, results are summarized and discussed.

2. Data and Methods

2.1. Numerical Modeling of Storm Surges and Waves

The generation and propagation of storm surges and wind-waves over the Mediterranean Sea originating from medicane events have been simulated using the fully coupled hydrodynamic and wave model SCHISM (Zhang et al., 2016), an upgraded version of the original SELFE model (Zhang & Baptista, 2008). The model is run in its 2DH barotropic mode fully coupled with the spectral wave model WWM-III (Roland et al., 2012). Both modules share the same unstructured grid covering the whole Mediterranean basin, with a closed boundary at the Strait of Gibraltar. The latter plays a key role in water exchange between the Mediterranean Sea and the Atlantic Ocean. Previous studies showed that subinertial flow through the Strait of Gibraltar is largely driven by atmospheric pressure over the Mediterranean Sea along with winds on the Atlantic side of the strait, and lead to Atlantic-Mediterranean sea level differences (Candela, 1991; García Lafuente et al., 2002; Le Traon & Gauzelin, 1997; Menemenlis et al., 2007). Therefore, closing the Strait of Gibraltar is a potential source for unmodelled signal within the Mediterranean Sea. We note, however, that the scope of this study is to simulate synthetic medicanes that provide atmospheric fields with a strong signal only in the vicinity of their tracks (see Section 5 and Figure 8). In this particular case, opening the domain toward the Atlantic and including the exchanges through Gibraltar Strait, would add negligible sea surface signals as no atmospheric perturbations would be applied in the Atlantic part of the domain. With our configuration only simulated changes in sea surface elevation controlled by the local effects of hydrostatic equilibrium (inverse barometer) and wind and wave setups from the medicane atmospheric perturbation are studied. Furthermore, although a closed boundary could lead to unrealistic accumulation of water under the influence of Medicanes traveling in the vicinity of the Strait of Gibraltar, these extratropical cyclones hardly reach the Alboran sea (see Section 3).

With a total of 36,078 nodes shared by 62,415 elements, the unstructured computational mesh has a horizontal grid resolution varying from ∼50 km in the open ocean down to ∼2 km at the coast. The EMODnet (Bathymetry, 2018) has been used with a grid resolution of 1/16 × 1/16 arc min (∼115 × 115 m). The computational time step is 10 min and outputs are saved every hour at all grid points. The surface wind stress is computed using a bulk formula of the drag coefficient following Pond and Pickard (2013). The bottom friction in the model is handled by estimating the bed shear stress with the Manning approach, assuming a value of 0.02 for the Manning friction coefficient. In the Mediterranean Sea, extreme coastal sea levels are mainly caused by storm surges rather than by the combination of tides and surges (Marcos et al., 2009). Furthermore, only the sea surface variability caused by medicanes is studied (meteorological sea surface variability), and therefore tides are not considered. The total wave spectral energy is distributed over 24 frequencies and 36 directions ranging from 0.04 to 1 Hz and 0–360°, respectively.

2.2. Data Used to Simulate Observed Medicanes

For the simulation of real medicanes, mean sea level pressure and surface wind fields for the duration of every medicane were obtained from ERA5 reanalysis data set (Hersbach et al., 2020), with a 0.25° spatial resolution and a 1 hr temporal resolution. For the validation of the model, tide gauge records were obtained from the Global Extreme Sea Level Analysis (GESLA) data set (Woodworth et al., 2016), that span the period until 2015 to compare for medicanes Querida and Rolf. For the most recent events, tide gauge data from the Copernicus Marine Environment Monitoring Service (CMEMS, https://marine.copernicus.eu/) and the Sea Level Station Monitoring Facility (http://www.ioc-sealevelmonitoring.org/) were used. As these services provide the complete sea level signal, the annual mean from observed sea levels was removed to avoid contributions from low-frequency sea level changes unrelated to extreme episodes. Moreover, the tidal signal was removed by using the python package pytides (https://pypi.org/project/pytides/) for the computation of tides. Modeled time series of H_s were compared to wave buoys from CMEMS.

2.3. Original Synthetic Medicane Data Set

With an average number of two or less events per year, the number of recorded medicanes is insufficient to perform robust statistics. We therefore used the outputs of Romero and Emanuel (2016) obtained through a novel statistical-deterministic approach that generates thousands of synthetic medicane tracks from atmospheric fields. This method, originally developed by (Emanuel, 2006) for tropical cyclones, accounts for the particular

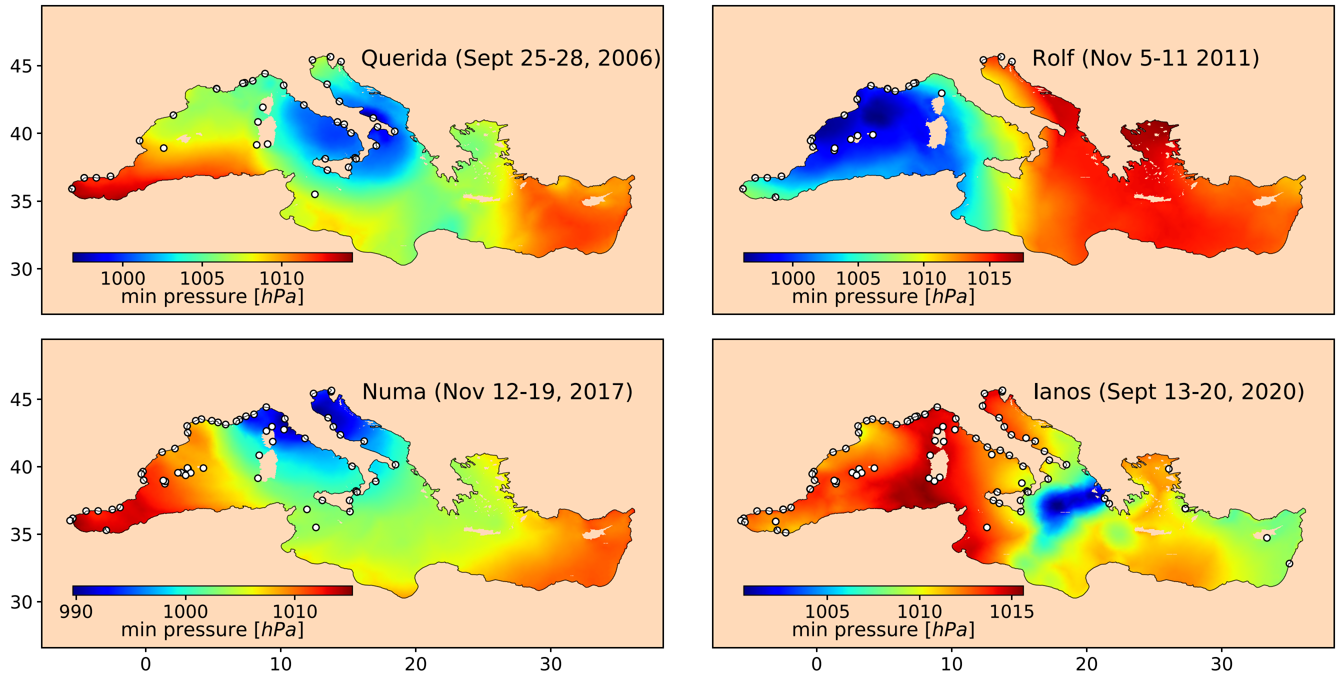

Figure 1. Minimum values of mean sea level pressure (from ERA-5 reanalysis) at every grid point corresponding to four medicanes used in the model validation. Also shown are the tide gauge locations.

characteristics of Mediterranean perturbations (Romero & Emanuel, 2013). The synthetic medicane data set consists of around 6,000 tracks derived from each of two atmospheric reanalyses (REAs), namely ERA-INTERIM and NCEP-NCAR, and 6,000 tracks for each run of 30 atm ocean general climate models (GCMs) from the Phase 5 of the Coupled Model Intercomparison Project (CMIP5); the latter runs include both historical and RCP8.5 simulations for 1986–2005 and 2080–2100 periods, respectively; that is, there are 12,000 tracks for each model. Out of the initial 30 climate models, the 20 models that best reproduced medicane track densities generated from the two reanalyses over the same period were kept (Romero & Emanuel, 2016). Since our work focuses on the Mediterranean basin, only those medicanes whose position during the time of highest intensity was located within the domain were retained. Therefore, tracks over the southeast of the Atlantic were filtered out along with all storms over the Black Sea. As a result, the frequency of medicanes toward the end of the 21st century found in Romero and Emanuel (2016) decreases from 200 to 180 per century. This is in agreement with the projected increased occurrence of medicanes in the Black Sea (Romero & Emanuel, 2016). The number of medicane tracks was reduced to an average of 3,000 per model run.

3. Model Validation With Ocean Observations During Medicane Events

The skills and performance of the model to reproduce the ocean response to medicane forcing are investigated on the basis of four historical observed events, namely Querida, Rolf, Numa and Ianos (see Table 1 for details of each event, including dates, duration, and intensity). For each run, both modeled storm surges and significant wave height (H_s) have been compared with in situ observations from coastal tide gauges and wave buoys, respectively. The number of in situ data locations used for each event are summarized in Table 1. Time series of the closest model grid point to each observational site, either tide gauge or buoy, were extracted for the comparison.

Figure 1 shows the minimum atmospheric pressure reach at each grid point from ERA5 reanalysis during the medicane event, together with tide gauge stations available during the cyclone life. In all cases, there are tide gauge observations in the vicinity of the center of action of the medicane. Since the numerical runs cover the whole Mediterranean basin, all available tide gauge records were used for the model validation in a first step, whether close or far from the medicane center, in order to check the consistency of the regional coastal elevation. Results show good agreement between modeled and observed coastal sea surface elevation for all medicane simulations, with a global root mean square error (RMSE%) reaching 3.2 cm (18.1%), 4 cm (13.6%), 2.9 cm

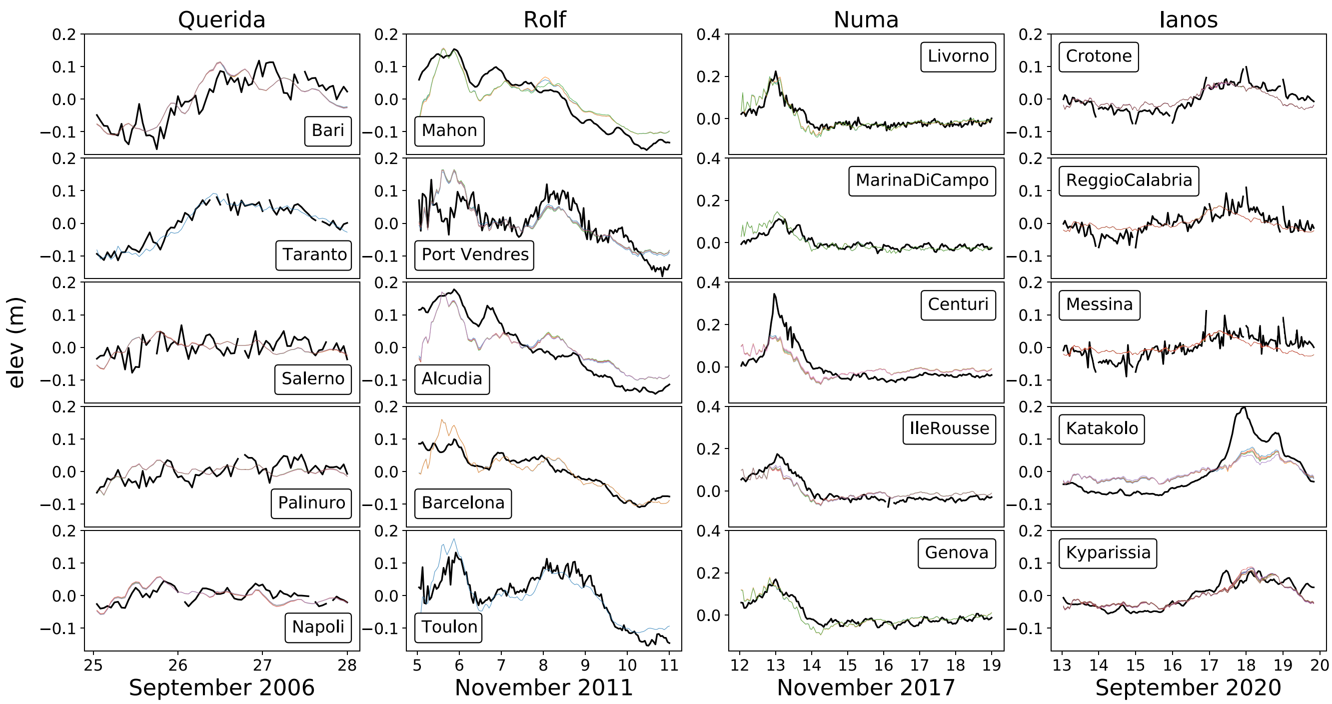

Figure 2. Validation of modeled sea surface elevation (colored lines) against observed sea surface elevation (black lines) for the five closest tide gauges to the minimum mean sea level pressure registered. The different colored lines correspond to grid points within 5 km from the tide gauge.

(14.9%), 1.8 cm (17.1%), and mean correlations of 0.63, 0.72, 0.45, 0.59, for Querida, Rolf, Numa, and Ianos, respectively. Additionally, the correspondence between model outputs and data has been investigated in detail for the five closest tide gauges to the minimum pressure point for each medicane. Results are shown in Figure 2. For every simulation, sea surface elevation mimics the oscillations of tide gauge signals and reproduces well their magnitude, including for the strongest events (Rolf, Numa, see Figure 2). The largest difference is found during medicane Ianos at Katakolo tide gauge and medicane Numa at Centuri tide gauge (12.5 and 17 cm underestimation at peak elevation, respectively). In this case, H_s higher than 4 m are found to propagate, with perpendicular direction, toward the coasts where the Centuri and Katakolo tide gauges are located. The sea surface elevation underestimation could be related to an underestimated wave setup due to the combination of the limited spatial resolution of 2 km at coast and the narrow continental shelf (discussed further in Section 6). In the rest of cases, simulated coastal elevation shows good agreement with tide gauge signals, with a RMSE (RMSE%) 2.3 cm (15.6%), 3.2 cm (11%), 2.4 cm (9.2%), 2.2 cm (13.5%), and mean correlations of 0.56, 0.87, 0.75, 0.86, for Querida, Rolf, Numa, and Ianos, respectively. The relative RSME decreases between 2.5% and 5.7% when only the five closest tide gauges are considered. We thus conclude that the simulations perform well and properly reproduce the sea surface elevation changes in response to medicanes, supporting the application of the current model configuration to a larger synthetic set of these extreme events (Romero & Emanuel, 2016).

As for sea surface elevation, H_s simulated during the four medicanes is compared to in situ wave buoy observations in Figures 3 and 4. Again, observations over the whole basin are used to check the regional consistency of results. Maps in Figure 3 show that at least one (for medicane Ianos) or several (for the other three medicanes) buoys were available in the area of highest waves. It is worth noting the large H_s ranges from 4.5 m to almost 7 m (the latter corresponding to medicane Numa). Comparisons between modeled and observed H_s show good agreement for all medicanes with a coefficient of determination varying from 0.81 to 0.91 and a RMSE of 13–25 cm (the largest value corresponding to medicane Numa that presents also largest H_s). Linear regressions in Figure 3 indicate that the model slightly underestimates observed waves. Figure 4 shows the simulated and observed H_s evolution at the five closest wave buoy locations to the maximum H_s. In line with the results shown in Figure 3, the model captures well the magnitude and variation of Hs for all four cases. During medicane Querida, however, wave observations near Palamós (A) and Barcelona (B) buoys display large differences with the model outputs in the earliest period; that can be explained by the combination of the spin-up effect and atmospheric disturbance

10.1029/2021JC017964

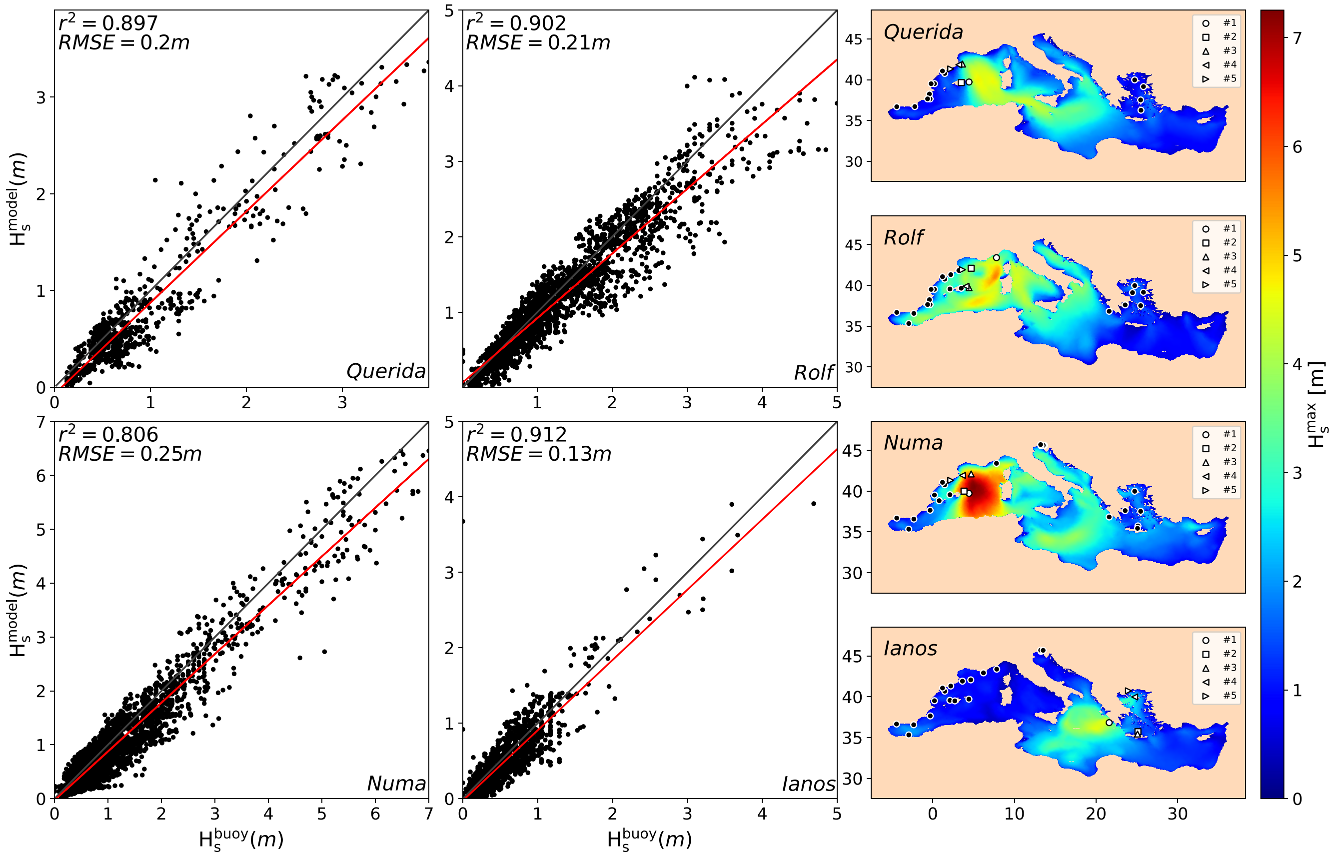

Figure 3. Comparison of H_s modeled and observed (left panels). Red lines in each panel represent the linear regressions (with slopes varying between 0.86 and 0.94); in black the 1:1 lines. Right panel: Maximum H_s at every grid point and wave buoy location (black dots). The position of the five closest buoys to the location of the maximum simulated H_s is referred to in the legend.

that preceded the cyclone perturbation. Furthermore, as stated above, the model shows an overall underestimation of H_s, but particularly when waves are higher. Amores et al. (2020) simulated the extratropical storm Gloria (January 2020, H_s up to 8 m) over the western Mediterranean and found the same levels of underestimation in H_s. It was attributed to the limited accuracy of the bathymetry and to small mismatches in the atmospheric forcing fields preventing the wave growth. In our case studies, Figure 4 shows that the greatest H_s underestimations occur at the time of highest waves at depths greater than 30 m (deeper than depths inducing wave breaking). Therefore, rather than bathymetry resolution, it is likely related to the resolution of wind forcing, which is a main source of errors for wave models (Bertotti & Cavaleri, 2009), and to the reported underestimation of wind speed by the ERA5 reanalysis data set (Kalverla et al., 2020), especially in areas with increased orographic complexity (Jourdier, 2020).

It is worth recalling that the model configuration with a 2 km spatial resolution along the coasts does not intend to resolve all physical processes at the coast but only the most relevant. The previous results suggest that the model is able to reproduce the response of ocean coastal elevation and wave generation and propagation under medicane forcing at the Mediterranean basin scale.

4. Selection of Synthetic Medicanes and Simulation

4.1. Selection of a Subset of Medicanes

Modeling coastal impacts of the total amount of medicanes is unfeasible due to computational constraints. Therefore, we selected a subset of events ensuring representativeness of the original medicane distribution in terms of location and intensity. For each model, a sensitivity analysis was conducted on the number of storm tracks that is needed to ensure that the subset displays the same distribution of maximum (cyclone-relative) tangential wind

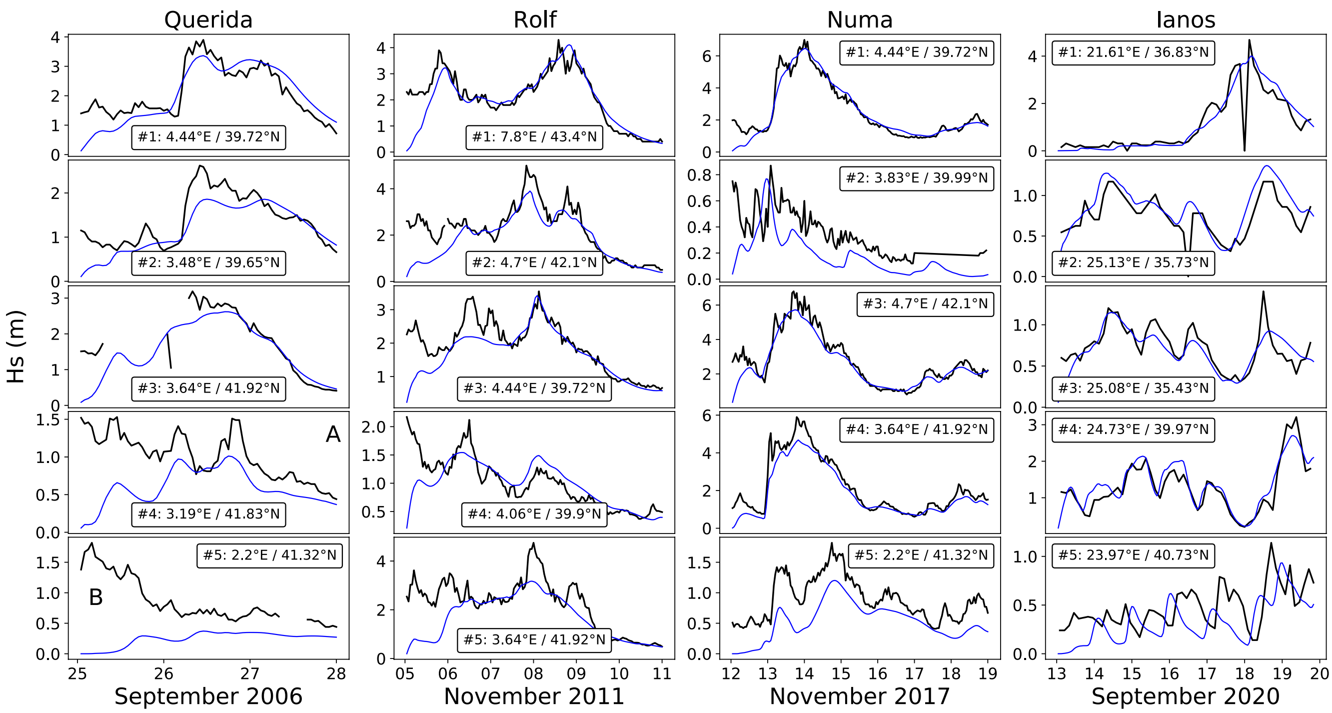

Figure 4. Validation of modeled H_s (blue line) against observed H_s (black line) for the five closest wave buoys (black line) to the location of maximum simulated H_s. Refer to Figure 3 for corresponding geographical position. For Querida storm, (a) and (b) represent, respectively, buoys near Barcelona and Palamós.

(S_{rot}). To that end, we built subsets of medicanes with sizes ranging from 10 to the total number of events in the model. In every subset, values of S_{rot} were randomly selected among those in the original distribution and this was repeated a hundred times for each subset size to strengthen the statistical analysis. Figure 5a shows the normalized probability density function (*nPDF*) of the original S_{rot} data set for one of the models and its comparison to the *nPDF* of generated subsets in terms of RMSE (b), correlation (c) and the *p* value of the Kolmogorov-Smirnoff test (d). Results indicate that a subset of 200 events (represented by the intersection of blue lines in Figures 5b–5d) is a good trade-off between the number of medicanes and its ability to replicate the statistics of the entire data set. Indeed, Figures 5b and 5c show that the correlation and RMSE converge toward 1 and 0, respectively, but very slowly for numbers larger than 200 events. Likewise, a Kolmogorov-Smirnov (K-S) test was performed between the original distribution of S_{rot} and the subset, ensuring that both come from the same continuous distribution. Therefore, the subset of 200 randomly selected medicanes with best statistical indicators was retained for each historical and projection run of the 20 climate models. For a better characterization of the present-day climate, a larger subset of 2,000 events were chosen for the two reanalyses. In a second step, in order to check the spatial representativeness of the subsets, their track densities were compared to the track density of the original distribution. This is done for coastal locations as these are the target of the present study. To do so, we considered that a coastal point located within the radius of a medicane (defined as the distance between the cyclone center and its band of strongest winds) at any time step of its lifetime is within its path. We then computed the percentage of the medicanes for every coastal point, represented in Figures 6a and 6b, averaged for the historical and projections runs respectively. Figures 6c and 6d map the differences (in percentage) between the densities in the original tracks and the selected subset. We found that for both historical and future periods, differences between the original and the subset distributions are on average very small with a mean value lower than 1%, and with an intermodel standard deviation of these differences of 2.5% at most, found in the central Mediterranean where medicane density is the highest. We thus conclude that the spatial distribution of the subsets is consistent with that of the original distributions.

Figures 6a and 6b also provide information on the spatial patterns of medicanes along the coastal regions. In agreement with Romero and Emanuel (2016), the highest medicane density is found in the central Mediterranean for both the original distribution (not shown) and our selection. The comparison between panels a and b also shows the projected decrease of track frequency in this region. Romero and Emanuel (2016) found that this

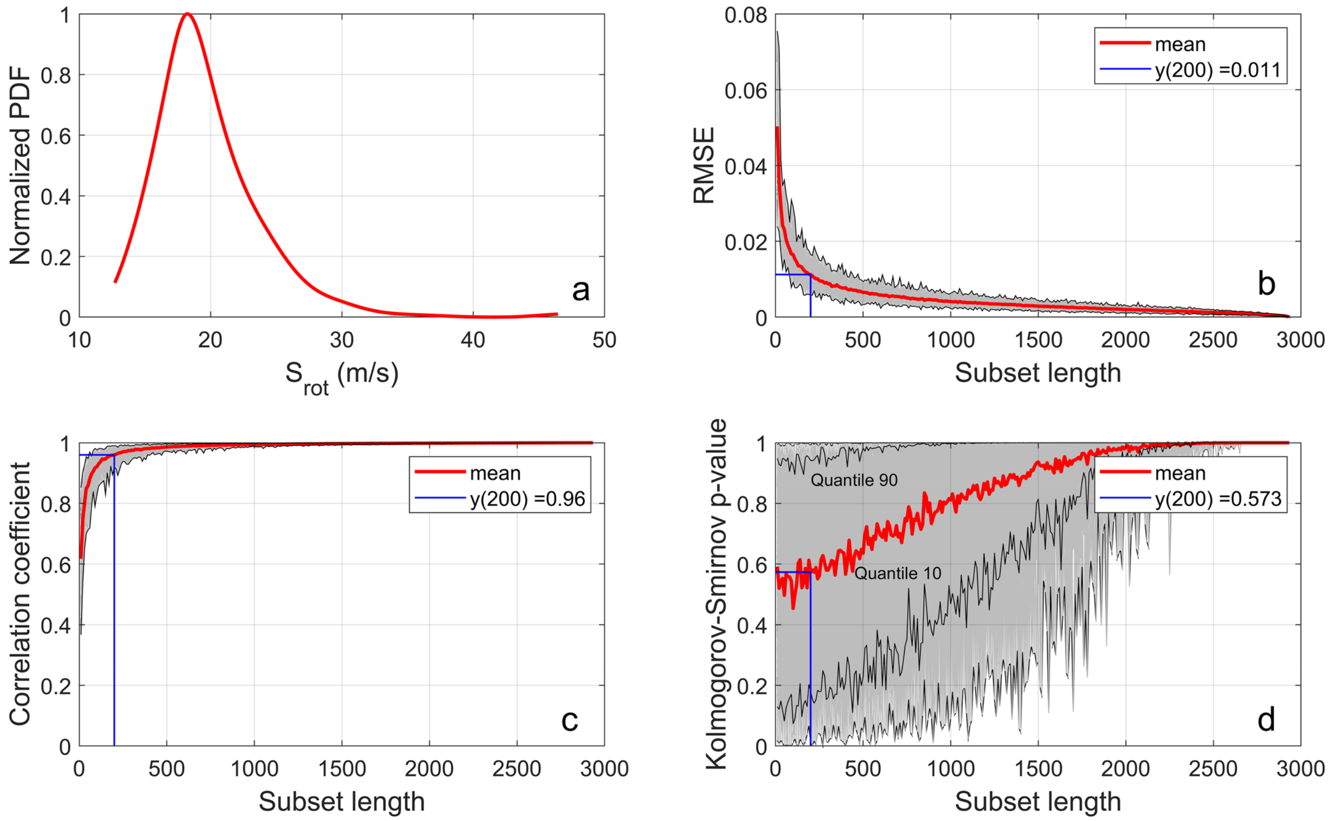

Figure 5. Sensitivity analysis on the S_{rot} parameter for the selection of synthetic medicanes. The *nPDF* of the original distribution (a, here GCMh16) is compared to *nPDFs* of randomly selected subsets using statistical indicators: RMSE (b), correlation (c), K-S *p* value (d).

predominant reduction of storm tracks in the central Mediterranean was balanced by an increased occurrence mainly in the Black Sea and, to a less extent, in the western Mediterranean. For the latter region, we report neither an increase in the subset nor in the original set, except for French coasts and particularly for the Balearic Islands. In addition, Romero and Emanuel (2016) concluded that medicane intensity is projected to increase by the end of the century and particularly for moderate and violent events. Figure 7 shows the median and the 75th and 95th quantiles of the S_{rot} within the 200 medicanes selection for historical and projections of every GCM model (Figure 7a). The results for the model ensembles are summarized in Figure 7b. In line with the results in Romero and Emanuel (2016), we find that the intensity, S_{rot}, increases in the projections with respect to the historical period especially for the 10 most intense storms (i.e., 95th quantile, as seen in Figure 7b).

We conclude that our selection of medicanes is consistent with the original data set in terms of location and intensity, and meets the main findings for the Mediterranean Sea from Romero and Emanuel (2016), which is a crucial step for the present work in order to assess the hazards induced along the Mediterranean coasts from medicane threats.

4.2. Numerical Simulations of the Ocean Response to Synthetic Medicanes

Atmospheric forcing fields corresponding to the subset of selected medicanes were used to simulate sea surface elevation and wind-waves in the Mediterranean, as described in Section 2. Figure 8 shows a snapshot of mean sea level pressure (a), wind speed (b), sea surface elevation (c), and H_s (d) for one of the selected synthetic medicane simulated. Top panels show the well-known near surface atmospheric structure of tropical-like cyclones in the Mediterranean (Emanuel, 2005; Patlakas et al., 2021; Toomey et al., 2019) with a low-pressure eye at the center and cyclonic winds. Higher winds (Figure 8b) are found at the medicane periphery, with larger values to its right due to the relative movement of the medicane. Bottom panels show the ocean response to the medicane forcing. A barometric inverse induced sea surface elevation at the center is observed (Figure 8c) and, as expected, generated

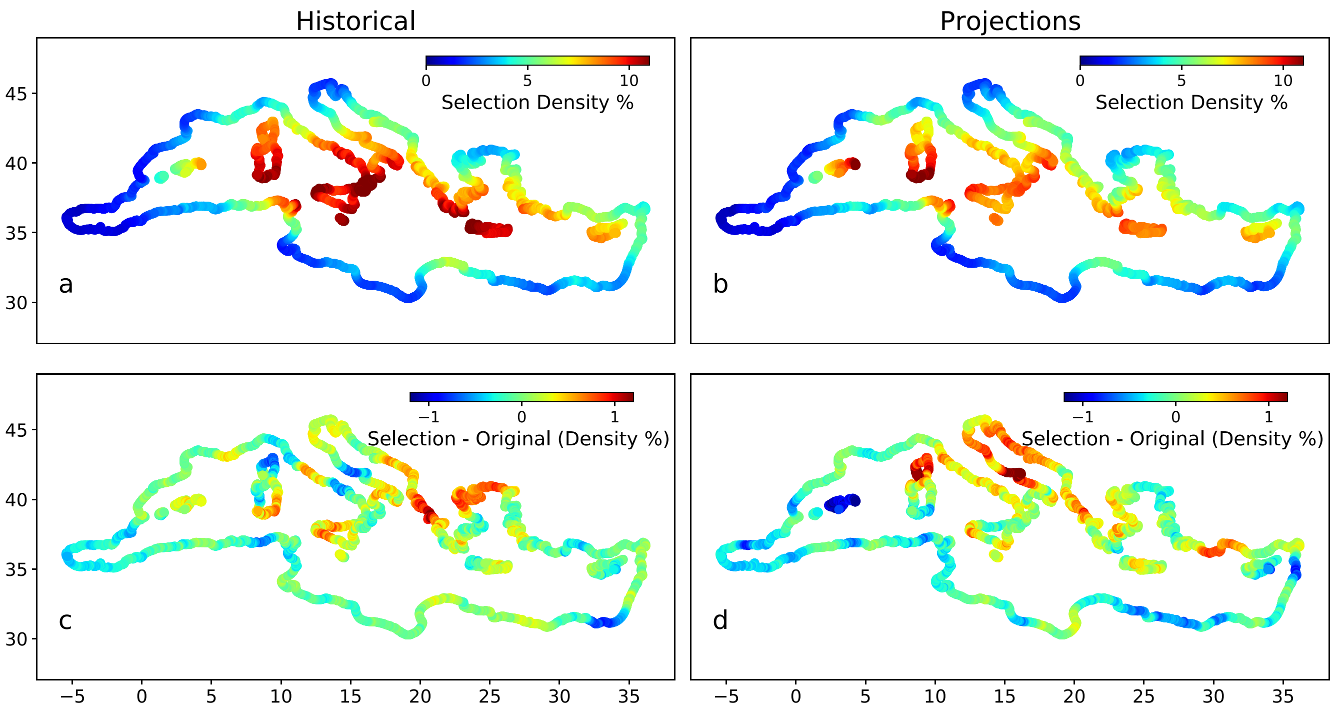

Figure 6. Spatial density patterns of storm tracks over the Mediterranean Sea for historical (a) and future projection (b) data sets of selected medicanes. Bottom panels show density differences (in %) with respect to the original distribution (c, d).

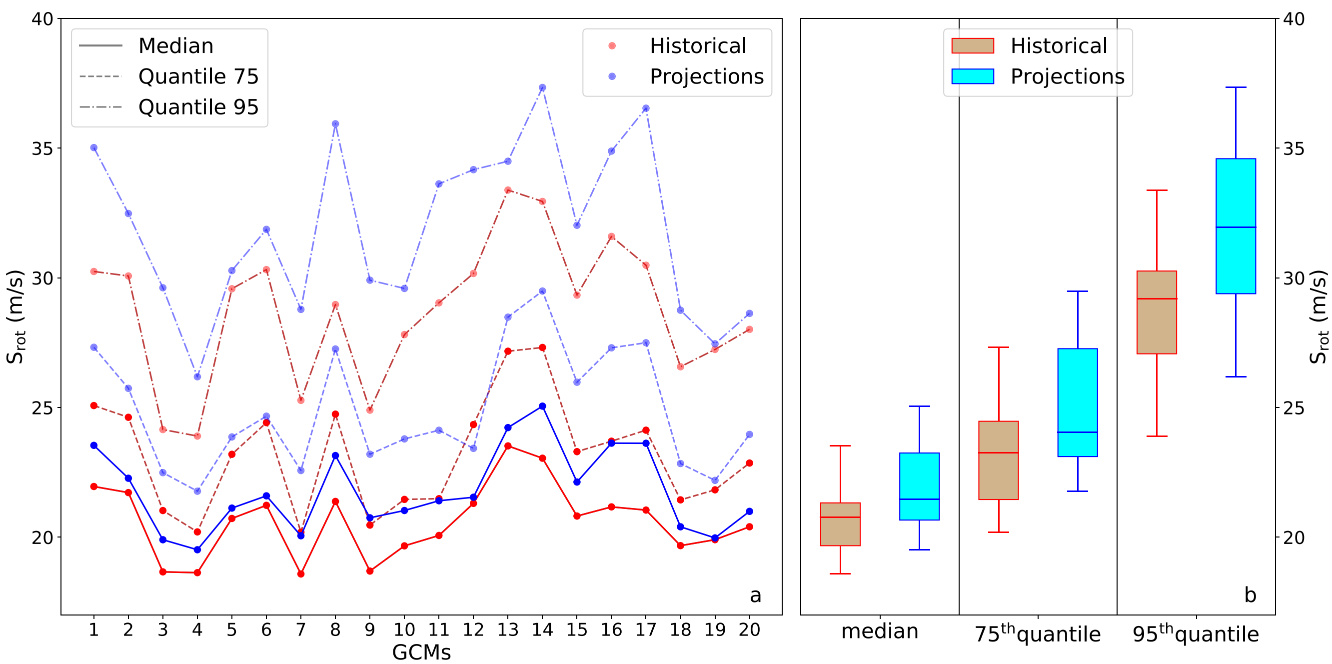

Figure 7. S_{rot} distribution of selected synthetic medicanes for historical and future periods. The median (continuous lines), 75th quantile (dashed lines), and 95th quantile (dashed-dotted lines) are represented for historical (red) and future (blue) period, for every model (a). The same information is depicted in the form of boxplots (b) in order to better visualize changes between historical (red) and projection (blue) S_{rot} distributions. Boxes extend from the first to third quartile values of the data, with a line at the median. Extreme whiskers show minimum and maximum values.

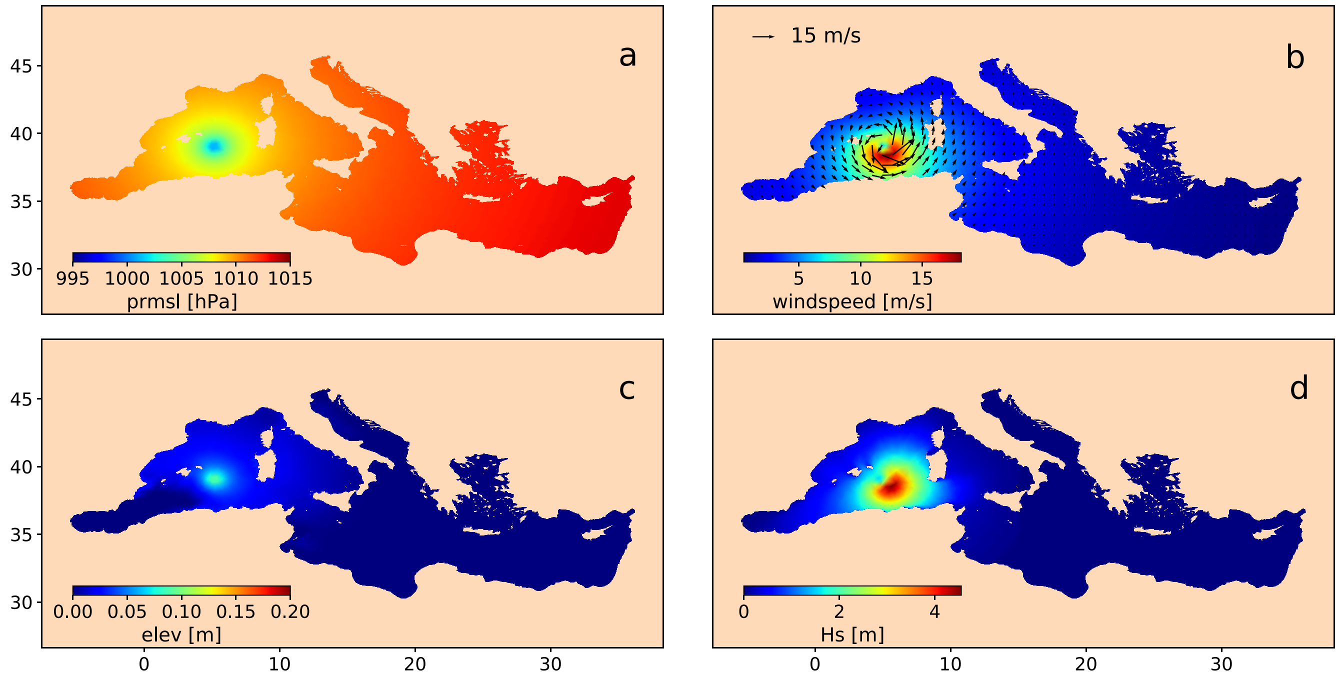

Figure 8. Example of atmospheric fields of mean sea level pressure and wind forcing during a synthetic medicane (a, b) and the corresponding simulated sea surface elevation and significant wave height (c, d).

waves are located where cyclonic winds are higher and their direction (not shown) follows the medicane path on its right side (in the southeast quadrant) with respect to track direction (i.e., northeastward in this case, Figure 8d), in agreement with Toomey et al. (2019) for the western Mediterranean.

The total set of 12,000 medicanes, including reanalyses, historical runs and projections, were simulated (computing time around 60 days with a 40 CPUs single node). For each medicane, maximum elevation and H_s registered at every grid point were retained, resulting in 200 (2,000) maps for every GCM (REAs) simulation. These model outputs are the basis for the characterization of the present-day ocean response to medicanes and its projected spatial and intensity changes. To extract the value along the coastlines in the case of waves, the value of H_s associated to each coastal grid point was chosen at the closest grid point at 20 m depth. This is because, at shallow depths, waves breaking induces wave setup which is already accounted for in the output of coastal sea level. Maxima values of H_s and elevation along the coastlines were used to compute return levels (RLs) of both variables for return periods varying from 10 to 100 years for each model. To that end, we fitted a Generalized Pareto Distribution (GPD) using the moment method (Hosking & Wallis, 1987), which has shown to be more reliable for sample sizes smaller than 500. The frequency of medicanes is therefore embedded into the RLs together with the intensity. However, all coastal points are not necessarily affected by all medicane-induced waves and storm surges. Therefore, in order to fit the GPD to our extreme events distribution, we discarded null values that are considered as residual and not medicane-induced (independently at each coastal point, for each model and for both H_s and elevation).

5. Ocean Response to Medicanes

5.1. Regional Wave Climate: Present-Day and Projections

The response of the regional waves to medicanes is displayed in Figure 9. Upper panels show H_s patterns for REAs simulations (4,000, accounting for both REAs) corresponding to the median, 75th and 95th quantiles (note the different color scales). Results highlight the predominance of medicane-generated waves in the central Mediterranean (between the islands of Lampedusa and Crete) where highest H_s is found with values reaching up to 15 m for 95th quantile, and the southeast part of the western Mediterranean. The very localized H_s medicane imprint for the median is representative of the strong medicane genesis in the central Mediterranean, as previously

10.1029/2021JC017964

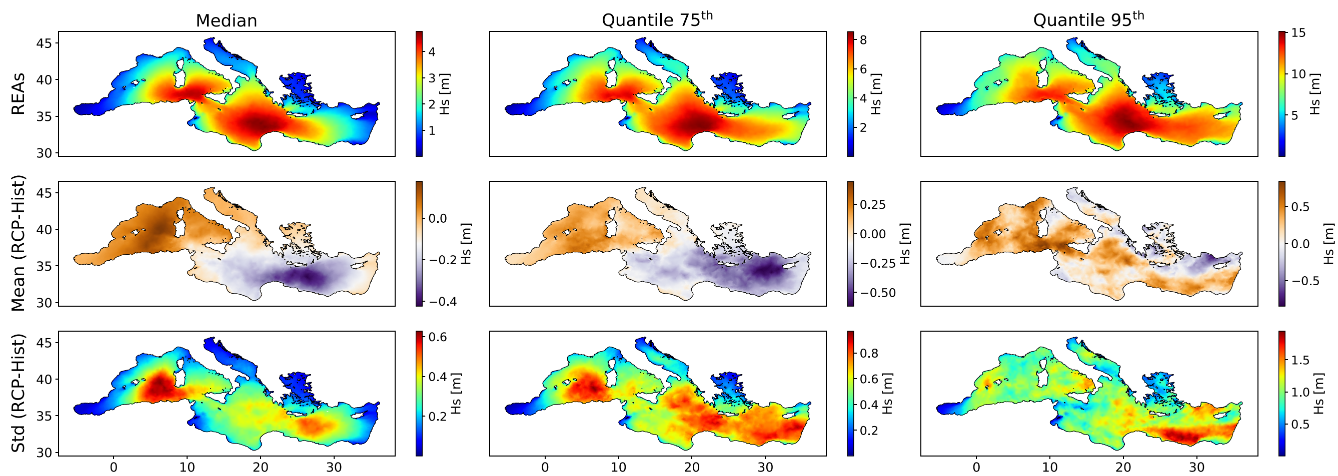

Figure 9. Medicanes induced wave climate for present-day and projected changes. Top panels show the spatial distribution of median H_s (left), 75th quantile (center), and 95th quantile (right) for the present climate (as given by reanalyses (REAs)). Middle row displays the mean of the 20 models differences between projections and historical runs (i.e., the projected changes), for the same three quantiles as in the upper row (50th, 75th, and 95th). Lower row maps the standard deviations of the means above.

mentioned. Nonetheless, it cannot be ruled out that waves generated remotely in a different basin may also reach the central Mediterranean, provided sustained intense winds occur (thus generating the necessary fetch). The opposite is observed in the northern Adriatic, the Aegean Sea or the Alboran Sea, where waves are limited by a short fetch and where smaller H_s are found also in response to a lower number of medicanes in these areas. It is worth noting that average events (represented by the median) are concentrated in the central Mediterranean with lower H_s close to the coastal regions in the western and eastern basins as well as in the Adriatic Sea; conversely, strongest events (as mapped in the 95th quantile) spread out in the entire basin, reaching most of the coastlines (with the exception of the Alboran Sea). However, independently of the statistical indicator used, the region of the Gulf of Gabes (eastern Mediterranean Sea, Tunisian coasts) concentrate very low values of H_s. In this area, wave growth is limited by extended shallow waters, that should induce wave setup as breaking depths are reached. As an order of magnitude, isobaths 50 m deep are reached 110 km offshore while depths of 200 m are not reached until 400 km from the coast (Othmani et al., 2017).

Middle and lower panels of Figure 9 map the same statistical indicators but referred to projected changes with respect to historical climate. These maps are produced computing the difference between the median, 75th and 95th quantiles of projected and historical wave patterns for each model (resulting in 20 fields of differences). Middle panels in Figure 9 show the mean of these differences, while lower panels display the standard deviations. Projected changes in the median H_s show a clear asymmetry between the western and eastern Mediterranean basins, with an increase in H_s up to 20 cm and a decrease of 40 cm, respectively. The same applies to the 75th quantile, although with larger projected changes reaching +45 cm in the western basin and −60 cm in the eastern basin. This result is in agreement with earlier findings reported by Romero and Emanuel (2016), who identified a reduction of medicane frequency in the central Mediterranean balanced by an increased of frequency in the western Mediterranean. We recall here that we also pointed out this increase in the western basin around the Balearic Islands (see Section 4). Changes in the 95th quantile of H_s (right column) represent variations of the most violent events. According to Romero and Emanuel (2016), these are projected to globally increase in wind speed, which explains the observed pattern in changes in H_s: an overall positive increase of up to 80–85 cm in the western and central Mediterranean. The only area with a projected decrease is located between Cyprus and south of Turkey, with values down to −85 cm, although very localized. Nevertheless, standard deviations around these averaged changes are overall large and specially in the southeastern part of the domain, suggesting that there is a lack of model consensus of the changes in the strongest medicanes toward the end of the 21st century.

5.2. Coastal Hazards

This section focuses on the impacts of medicane-induced waves and sea surface elevation along coastal regions. While the previous section provided information on the intensity of regional waves in response to medicanes, changes in their frequency reported in Section 2 are not accounted for. In order to incorporate both intensity and frequency changes, we computed return levels (RLs) for both elevation and H_s, as described in Section 4.2. For illustration purposes, we plot RLs of H_s and elevation along the continental coasts and along islands separately. We select return levels corresponding to 10-year and 100-year return periods and their changes under RCP8.5 climate change scenario by late 21st century. RLs are either mapped along the coastlines (for present-day values obtained from REAs) or plotted linearly with the abscissas representing the coastal point number. In the latter, Mediterranean coasts are split into eight continental zones and eight islands.

5.2.1. Present Climate

Figure 10a maps the 100-year RL of H_s induced by medicane activity along the Mediterranean coasts for present-day as provided by REAs. Results show that, for 71.4% (22.4%) continental coastal points, 100-year RL of H_s are greater than 5 m (9 m). These values increase for islands up to 93.2% for 100-year RL larger than 5 m and 30% for 9 m. The reason is their location with respect to the medicane generation area, that makes island coasts to be hit before continental coasts. The geographical distribution of the RL for H_s is consistent with the overall regional medicane-induced wave climate shown in Figure 9: highest H_s RLs are found for central-eastern Mediterranean in the southwest of Greece (coastline number 5 in the inset Figure 10c), northeast of Lybia (coastline number 7), northeast of Algeria and north Tunisia (coastline number 8) as well as along the western side of Crete Island. In these regions 100-year RL of H_s reaches up to 14.25 m. Likewise, values of close to 14 m are found along the west coast of Cyprus and the continental coasts of the eastern Mediterranean (from Israel up to Lebanon, zone 6). Conversely, lower H_s RLs are located in the regions with no medicane generation and expected to have small fetch (e.g., Alboran and Aegean Seas). It is worth noting that H_s values along the coast of Croatia (eastern Adriatic Sea) are very low in comparison to the significant wave height in other parts of this basin; this is because this coastline is protected by a belt of islands, that acts as a barrier stopping the high waves from reaching the continental coastline. This same effect is observed in the Aegean Sea where wave growth is limited by a smaller fetch area due to the numerous islands within it.

Panels in Figure 10d allow to compare 10-year and 100-year RLs of H_s for the continental coastlines while panels in Figure 11b correspond to island coastlines. Both curves display consistency for moderate and strong events in H_s. Besides the numbers for the strong events reported above, it is notable that moderate events, those occurring once in 10 years, reach H_s values higher than 4 m in all coastal areas and 8 m in northeast of Lybia (zone 7) and Crete island (G). This indicates a high probability of hazardous events associated with waves generated by medicanes in the short term.

Coastal sea surface elevation induced by medicanes is represented in Figures 12 and 13 along continental and island coastlines, respectively, in the same fashion as for H_s. Regional patterns in coastal sea surface elevation differ from those in H_s. Large values of coastal sea levels for both 10-year and 100-year RLs are found in the Adriatic Sea (zones 3 and 4), especially toward the northwestern region, with values exceeding 1 m. In this area, storm surges are often caused by Sirocco winds blowing from the southeast. Particularly, Venice and its surroundings are located at the end of the longest fetch of Sirocco induced by air-pressure gradients linked to Mediterranean low-pressure systems crossing the Adriatic sea (Medugorac et al., 2018). Here, medicane-induced winds from southeast generate extreme total water levels in the north of the Adriatic Sea in a similar way as prevailing Sirocco winds. In the southern and eastern Mediterranean, high values of medicane-induced coastal sea levels are also found in the Gulfs of Gabes and Syrte (zone 7, Lybian coasts) and around the Nile Delta (zone 6) with 100-year RLs between 0.4 and 1.35 m. These zones have in common wide continental shelves with mild slopes that favor wind and wave setup contributions to storm surges induced by medicanes. In shallow waters areas, the latter is well represented despite the coarse model resolution at the coast (2 km). Overall values are smaller and rather uniform in the western basin, not exceeding 0.7 m for 100-year RL in areas as the Gulf of Lion and the eastern Spanish coasts, also characterized by shallow continental shelves.

5.2.2. Projected Changes

Projected changes in 10-year and 100-year RLs of H_s under RCP8.5 by the end of the century are shown in Figures 10e and 11c for all coastal grid points. Projected changes were computed as the difference between projected and historical RLs for each individual GCM (note that medicane frequencies in historical runs are 2 events per year, while frequencies in projections depend on each model). Results are represented as the multi-model ensemble median (blue/red curve) and spread given by the 25th and 75th quantiles (shaded area). Also,

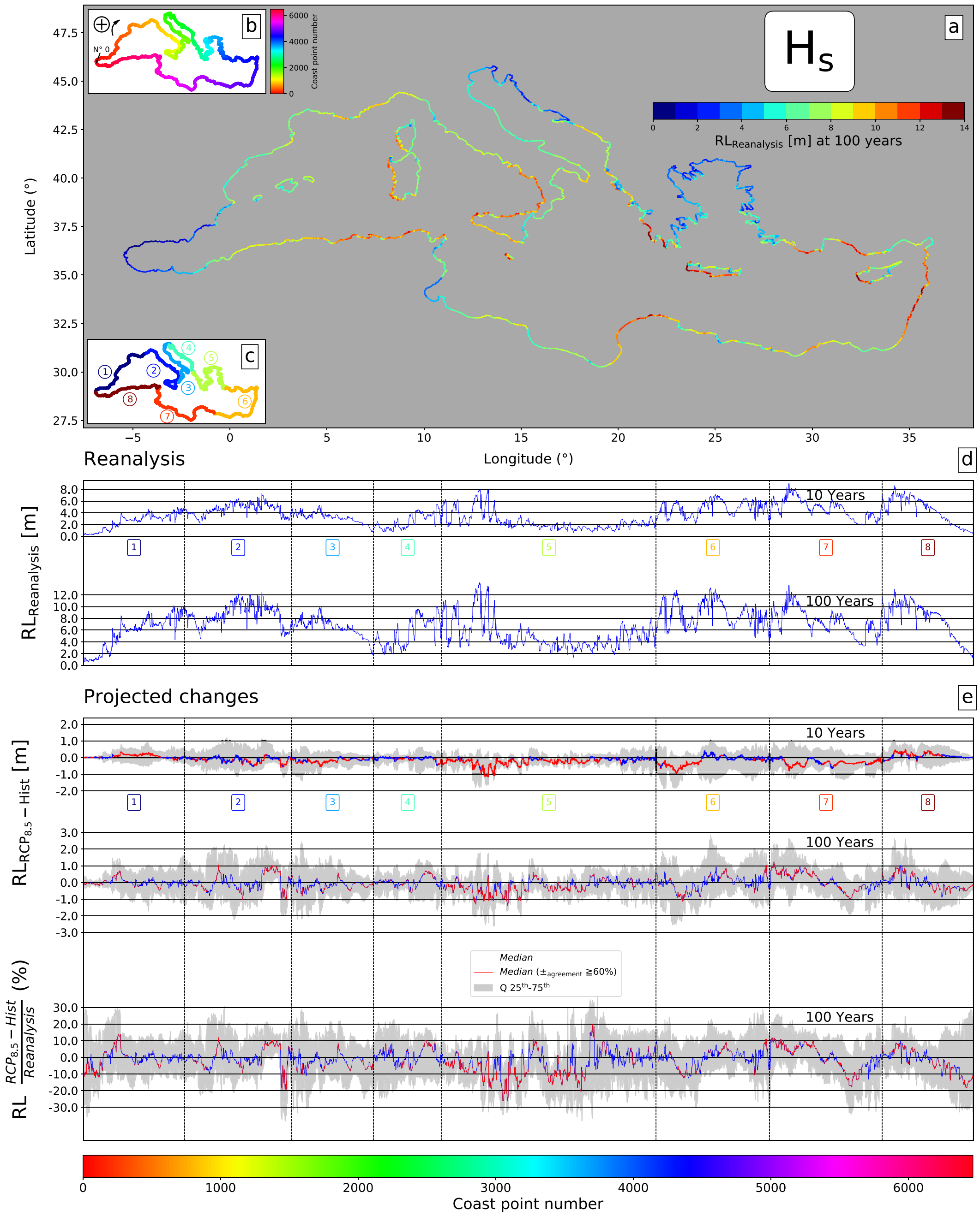

Figure 10. Medicanes induced return levels (10–100 years) of H_s for present and future climate along continental coasts. Top panel shows coastal regional return levels in the Mediterranean (a), coast point numbers (b) and coastal zone division (c). Middle graphic (d) shows reanalyses return levels. Lower graphic (e) shows projected changes in return levels for the median (either in blue or in red when at least 60% of models agree on sign of change) and the 25th–75th quantiles statistical indicators (shaded).

relative changes (in %) with respect REAs RLs are plotted in the bottom graph. Model agreement is shown as a red curve wherever at least 60% of GCM models agree on the sign of change, that is, either an increase or a decrease in the RLs in the future projections; otherwise the multimodel median is plotted with a blue curve. Changes in moderate events of H_s induced by medicanes, represented by its 10-year RL, are projected to decrease along most of the continental coasts (Figure 10e), with 75.1% of coastal points showing a reduction up to 1 m (concentrated in zones 5, 6, and 7), 41.4% with model agreement. Likewise, along islands coastlines (Figure 11c) the decrease in 10-year RL dominates with 73.1% of the coastal points (50.6% showing model agreement) and

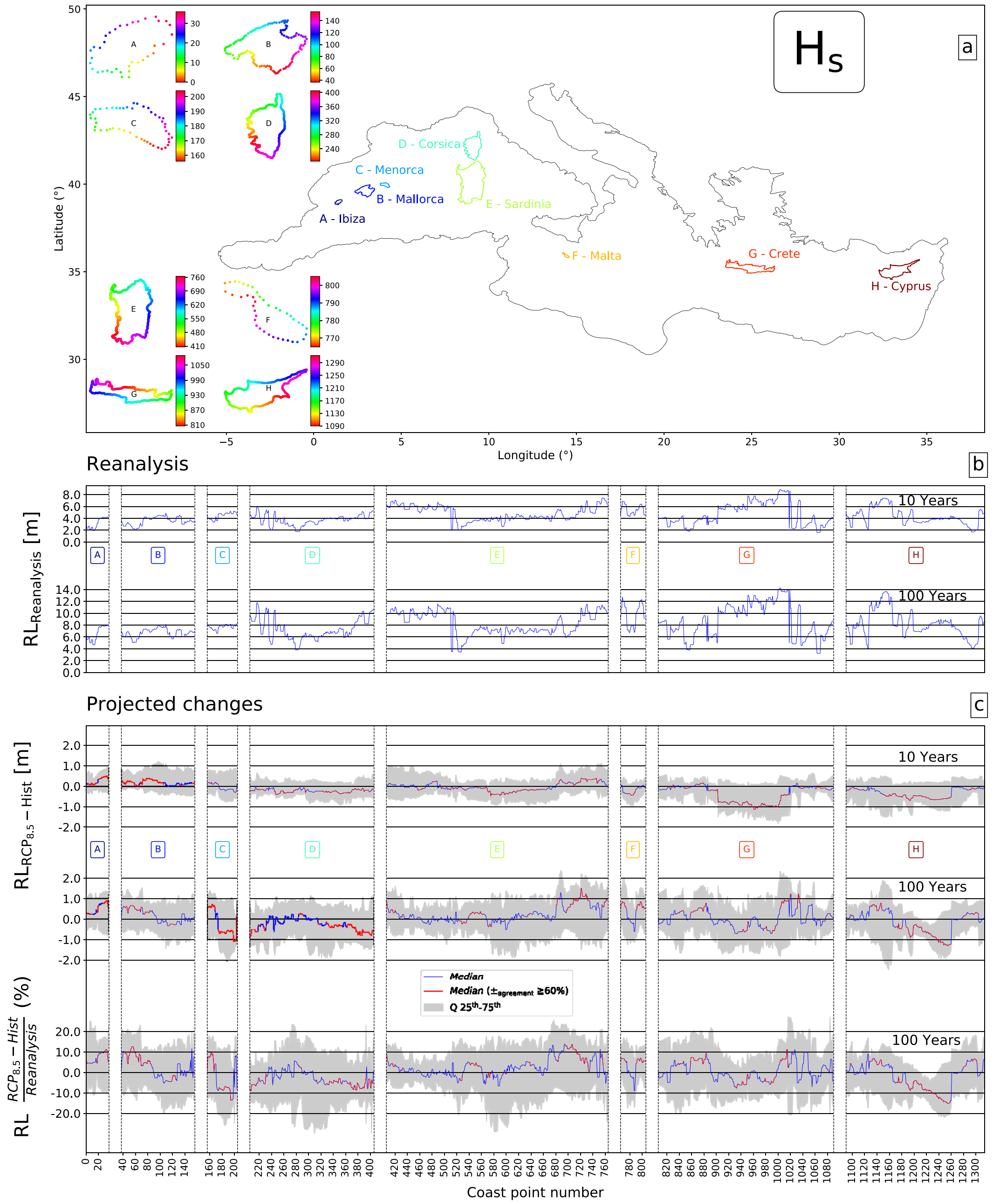

Figure 11. Medicanes induced return levels (10–100 years) of H_s for present and future climate in Mediterranean islands. Top panel shows islands studied. Middle graphic (b) shows reanalyses return levels. Lower graphic (c) shows changes in projected return levels for the median (either in blue or in red when at least 60% of models agree on sign of change) and the 25th–75th quantiles statistical indicators (shaded).

reaching values of 1.13 m for the south of Crete (island G). The exception to this decrease is found around the Balearic Islands (islands A and B) and the southern coasts of Sardinia (island E), showing an increase in 10-year RL up to 50 cm with model agreement.

Changes in 100-year RL, corresponding to the most intense events, behave differently to moderate events. Some coastal regions with projected increased H_s for strong events can be found. This is the case, for example, of southern Sicily (zone 2) with a projected increase of 1 m and model agreement up to 80%, contrasting with the absence of changes in the impact of 10-year RL events. This difference can be, at least in part, explained by projected decrease in the medicane frequencies combined the with projected rise in wind intensity associated to medicanes,

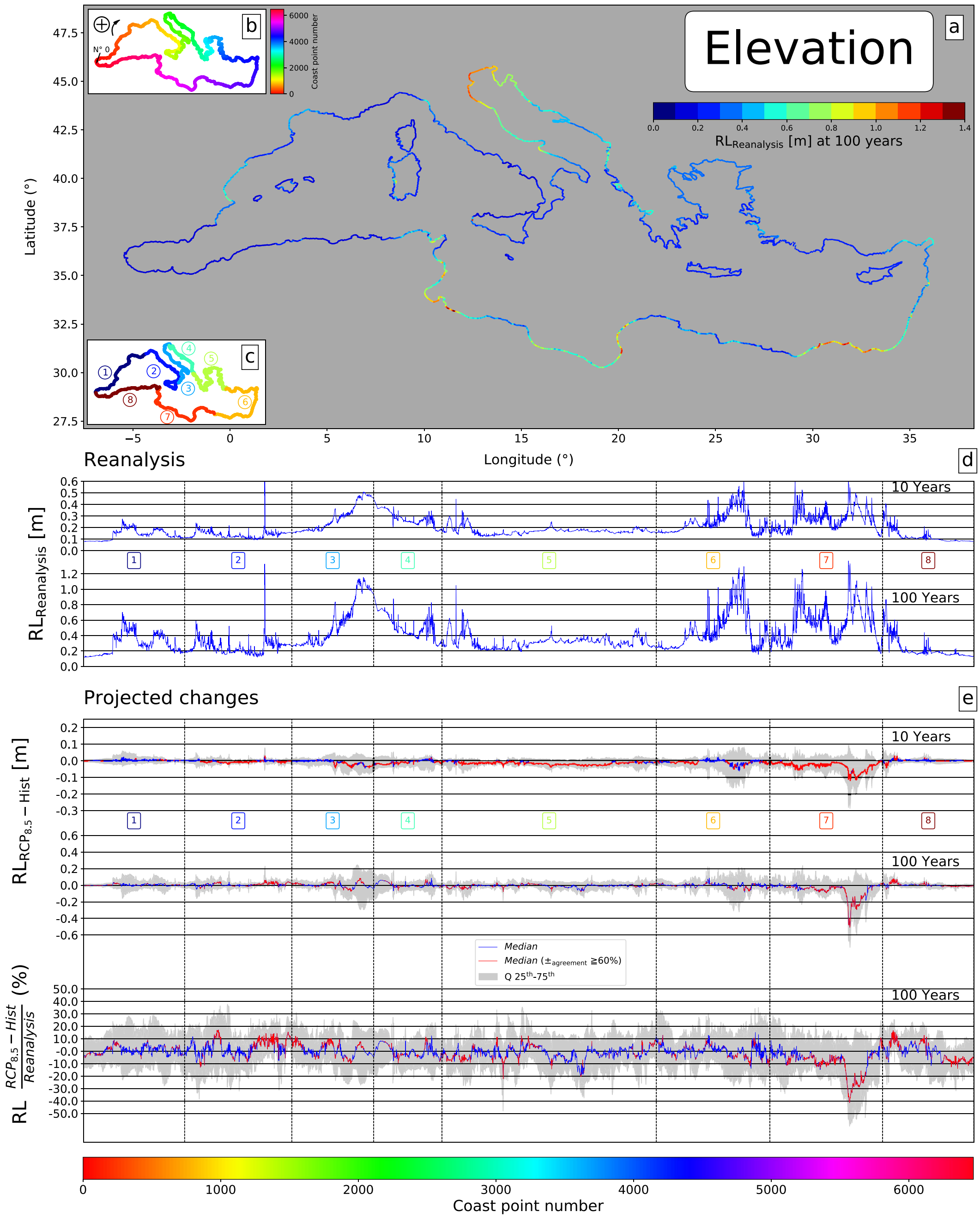

Figure 12. Medicanes induced return levels (10–100 years) of coastal elevation for present and future climate along continental coasts. Top panel shows coastal regional return levels in the Mediterranean (a), coast point numbers (b), and coastal zone division (c). Middle graphic (d) shows reanalyses return levels. Lower graphic (e) shows projected changes in return levels for the median (either in blue or in red when at least 60% of models agree on sign of change) and the 25th–75th quantiles statistical indicators (shaded).

as pointed out in Section 4.4.1. Overall, in 59.6% of continental coastal points, 100-year RLs of H_s are projected to decrease (29.8% displaying model agreement) and, similarly, 47% of coastal points in islands (with 23.2% of which show model agreement). These changes range between 0.2 and 1 m, except in southern Greece (zone 5), in eastern Sicily (zone 2) and in the region between Cyprus and Turkey (zone 6), with values exceeding 1 m. These values correspond to 15–25% relative changes with respect to REAs $RLs_{100\text{-}years}$ of H_s, as indicated in the bottom panels. Areas with projected rise in 100-year RL of H_s, in addition to the above-mentioned of Sicily, are located around the Balearic Islands with changes between 20 and 90 cm, Sardinia, Malta, Crete, Cyprus islands (E, F,

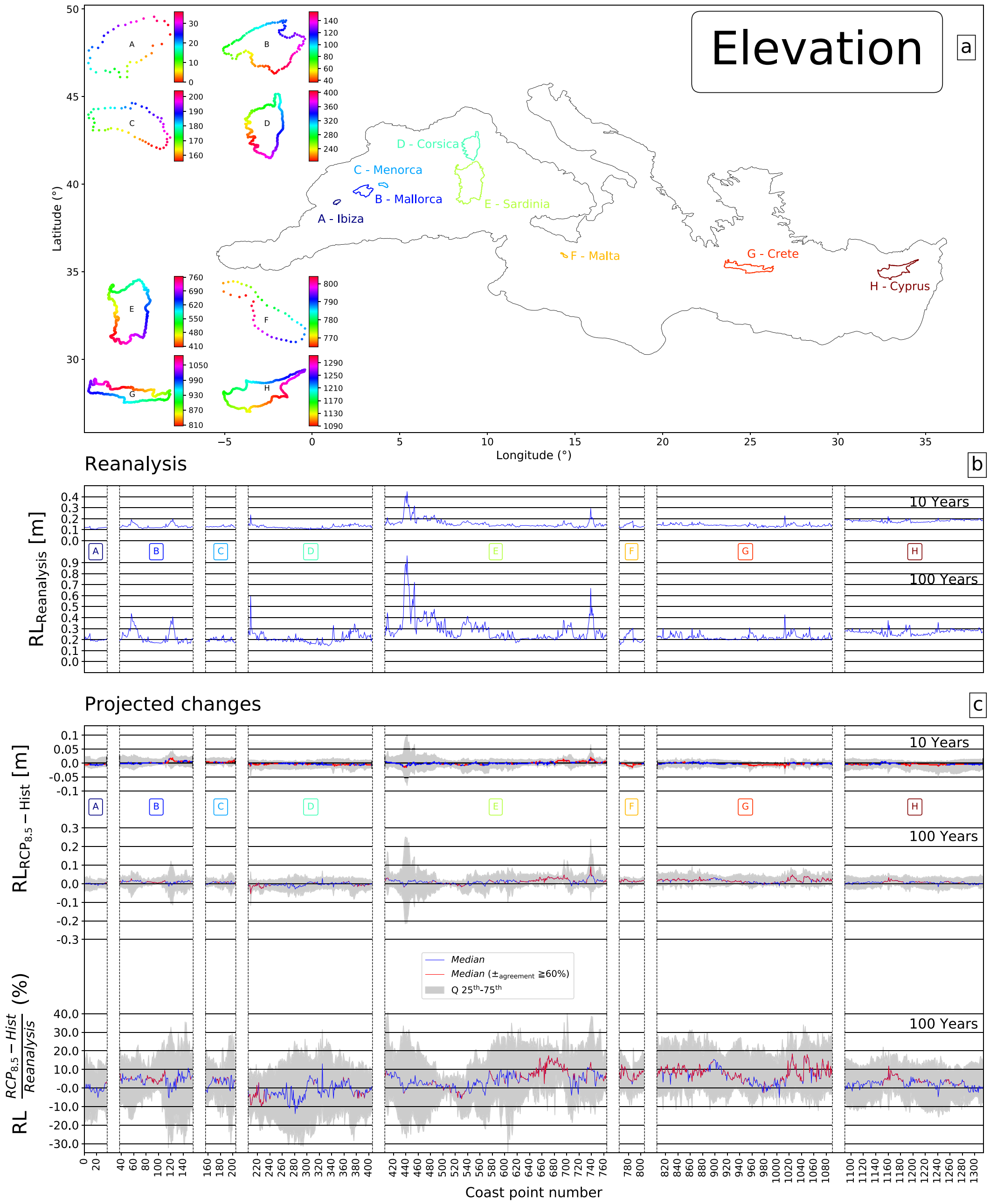

Figure 13. Medicanes induced return levels (10–100 years) of coastal elevation for present and future climate in Mediterranean islands. Top panel shows islands studied. Middle graphic (b) shows reanalyses return levels. Lower graphic (c) shows changes in projected return levels for the median (either in blue or in red when at least 60% of models agree on sign of change) and the 25th–75th quantiles statistical indicators (shaded).

G, and H) and the southeastern basin (zone 7) with up to 1.5 m increase (corresponding to 6–13% of relative changes). Notably, half (49.6%) of the total number of coastal points display multimodel agreement, a number that drops to 12.2% if the agreement is defined at the 70% of the models. This is illustrated by the relatively large dispersion in the quantiles (shaded areas).

Figures 12e and 13c show (in the same way as for H_s) projected changes in 10-year and 100-year RLs of coastal elevation. RLs found for both return periods exhibit, once again, different behavior, but in this case with relatively smaller amplitudes and with poorer intermodel agreement than for H_s. Projected changes in 10-year RLs of coastal elevation are negative along 80.4% of coastal continental points (with 54.4% exhibiting intermodel agreement) and 68% of coastal points of islands (30.3% with intermodel agreement). Although still with small changes, results for projected variations in 100-year RLs of coastal elevation show a different behavior: along continental coasts about half of the grid points show a decrease but with model agreement in only 25.4%. Likewise, in islands the results are also highly uncertain, with 20.6% of coastal points displaying negative changes and only 5.94% showing model agreement. In terms of magnitudes, projected changes are mostly of the order of a few cm. The exceptions are the northern Adriatic Sea (zone 3) with positive values between 5 and 10 cm (7–11% relative changes) and the Lybian coasts and Gulf of Gabes (zone 7) with −45 cm (40% relative decrease). In this area, this reduction is partly linked to the similar decrease in H_s that reduces the contribution of the wave setup. It is worth noting that only 45.8% of coastal grid points exhibit intermodel agreement, dropping down to 10% if the threshold for model agreement is set to 70% (not shown). There is therefore a limited model consensus in changes in coastal elevations induced by medicanes.

6. Summary and Discussion

Using a distribution of 4,000 synthetic medicanes, built from two atmospheric reanalyses, as the forcing of a coupled hydrodynamic-wave ocean model, we produced a robust assessment of medicane-induced coastal hazards along Mediterranean coastlines. In parallel, potential future changes were investigated by numerically simulating the ocean response to 12,000 synthetic medicanes derived from 20 GCMs for both historical simulations and future projections for the late 21st century under the RCP8.5 climate scenario. Ten-year and 100-year return levels were computed for two variables, namely H_s at 20 m depth and coastal sea surface elevation every 2 km, showing spatially and temporally varying intensities, thereby identifying the regions exposed to medicane impacts and its projected changes.

Medicane-induced large wind-waves have the potential to impact the majority of the Mediterranean coasts, except those located in areas of limited potential fetch (Alboran Sea, Adriatic, and Aegean seas) and those protected by wide natural barriers (like the Dalmatian coasts in the Adriatic). Indeed, almost three out of four coastal points face 100-year RL of H_s greater than 5 m, and even higher in the western and mainly central Mediterranean (around the Ionian sea). These results are in agreement with Patlakas et al. (2021), who recently simulated 40 documented medicanes that occurred over a period of 25 years (an average rate of 1.6 events/year), although they identified mainly the western Mediterranean coasts as the most exposed to medicane-induced waves and, to a lesser extent, the central basin. Other recent works focusing on regional wave climate (not only on medicanes) are also consistent with respect to the areas with higher exposure, based on either in situ observations or numerical hindcasts (Elkut et al., 2021; Morales-Márquez et al., 2020; Soukissian et al., 2017). Large values of H_s were also obtained in areas of high potential fetch such as the Gulf of Lion, the Algerian basin and, to a lesser extent, the Tyrrhenian Sea which are exposed to north-westerly mistral winds (Menéndez et al., 2013).

In contrast to the spatial patterns of highest waves, largest values of medicane-induced coastal sea surface elevations are found in the northern Adriatic Sea (caused by storm surges induced by southeasterly wind setup effect) and in regions with wide shallow continental shelves (Gulfs of Gabes, Syrte, Nile delta, Gulf of Lion, and the Spanish eastern coasts) that favor wind and wave setup. In these shallow areas, wind effect becomes dominant over inverse barometric effect for storm surges generation (Bertin et al., 2017). However, away from gently sloping continental shelves, the coastal resolution of 2 km is insufficient to properly capture the wave setup in the model (as seen for the tide gauge in Centuri during Numa medicane in Section 3). In these regions with small or no continental shelf, the wave setup is expected to be an important contributor to coastal sea level extremes when waves hit normal to the coast, while wind contribution is often very weak (e.g., Kennedy et al. (2012) for the case of volcanic islands). Therefore, with the current grid configuration, wave setup is very likely underestimated. Overall, our results of medicane-induced perturbations over the ocean surface point out that different physical processes that contribute to coastal sea level extremes are not spatially correlated (barometric atmospherics, wind and wave setup) and dominate in different regions depending on their morphological configuration and location within the basin. Such differences are relevant to properly identify the associated coastal hazards and derive the risks to be accounted for by economic and social stakeholders.

With respect to projected changes of medicane-induced coastal hazards toward the late 21st century, there is limited multimodel agreement in terms of magnitude and even sign of the projected changes along most of the coastal regions. For H_s, only less than half of the coastal grid points display 60% model agreement on the sign of change of the 100-year RL; a few locations (e.g., north Mallorca and Ibiza islands, north Algeria and Tunisia, south Sicilia, Malta, north Lybia, south Greece, Crete island, Turkey, Cyprus island) have a good model consensus (60–80%), although relative changes do not exceed 20% of the present-day value. Interestingly, when moderate (10-year RL) and strong (100-year RL) events for H_s are compared the behavior can be opposite, reflecting the effect of projected future increased medicane intensity. The most glaring example is the case of south of Sicily: from a projected decrease in 10-year RL to a projected increase in 100-year RL with values higher than 1 m and with significant model agreement. For coastal sea surface elevation, the multimodel spread is even higher than for H_s. Except for very specific regions (Gulf of Gabes and Northern Adriatic), projected changes of storm surges are very low and display poor model consensus. This reflects the dispersion of atmospheric models as already pointed out in Romero and Emanuel (2016) (see Table 1). Such small changes and their uncertainties are consistent with earlier studies that investigated the future storm surges in the Mediterranean Sea and found insignificant changes or even decreases in some regions (Androulidakis et al., 2015; Conte & Lionello, 2013; Jordà et al., 2012; Marcos et al., 2011; Muis et al., 2020; Vousdoukas et al., 2016, 2017).

To our knowledge, this work represents the first complete assessment of coastal hazards induced by medicanes along the Mediterranean coasts. Taking advantage of existing databases of synthetic medicane tracks that are consistent with current and future projected climate, we have modeled the hydrodynamic and wind-wave response of the ocean. Our method reduces the number of atmospheric events ensuring consistency with the original distribution of synthetic medicanes, in order to make the oceanic modeling feasible within a short period of time (days to weeks) with standard computational capabilities. This methodology can be easily extrapolated to other regions facing impacts derived from cyclonic disturbances, provided the information on the atmospheric events is available, without requiring high computational resources.

Data Availability Statement

Return levels at 10-year and 100-year periods for the present climate and projected changes for both H_s and coastal elevation are available at the Zenodo repository with identifier https://doi.org/10.5281/zenodo.5723461.

Acknowledgments
This study was supported by the Project RTI2018-093941-B-C31 funded by MCIN/AEI/10.13039/501100011033/ and by FEDER Una manera de hacer Europa. Tim Toomey acknowledges an FPI grant associated with the MOCCA project (Grant No. PRE2019-088046). Angel Amores was funded by the Conselleria d'Educació, Universitat i Recerca del Govern Balear through the Direcció General de Política Universitària i Recerca and by the Fondo Social Europeo for the period 2014–2020 (Grant No. PD/011/2019). Marta Marcos was supported by the Ministerio de Ciencia e Innovación and la Agencia Estatal de Investigación through Grant No. IED2019-000985-I. Romu Romero was funded by FEDER/Ministerio de Ciencia, Innovación y Universidades—Agencia Estatal de Investigación through the COASTEPS project (Grant No. CGL2017-82868-R).

References

Amores, A., Marcos, M., Carrió, D. S., & Gómez-Pujol, L. (2020). Coastal impacts of storm gloria (January 2020) over the north-western Mediterranean. *Natural Hazards and Earth System Sciences*, *20*(7), 1955–1968. https://doi.org/10.5194/nhess-20-1955-2020

Androulidakis, Y. S., Kombiadou, K. D., Makris, C. V., Baltikas, V. N., & Krestenitis, Y. N. (2015). Storm surges in the Mediterranean sea: Variability and trends under future climatic conditions. *Dynamics of Atmospheres and Oceans*, *71*, 56–82. https://doi.org/10.1016/j.dynatmoce.2015.06.001

Bakkensen, L. (2017). Mediterranean hurricanes and associated damage estimates. *Journal of Extreme Events*, *4*, 1750008. https://doi.org/10.1142/S2345737617500087

Bathymetry, C. E. (2018). *Emodnet bathymetry consortium (2018). Emodnet digital bathymetry (dtm 2018). Emodnet bathymetry consortium*. https://doi.org/10.12770/18ff0d48-b203-4a65-94a9-5fd8b0ec35f6

Bertin, X., Olabarrieta, M., & McCall, R. (2017). Hydrodynamics under storm conditions. In P. C.et Giovanni Coco (Ed.), *Coastal storms: Processes and impacts*. John Wiley & Sons Ltd. Retrieved from https://hal-univ-rochelle.archives-ouvertes.fr/hal-01671860

Bertotti, L., & Cavaleri, L. (2009). Large and small scale wave forecast in the Mediterranean sea. *Natural Hazards and Earth System Sciences*, *9*(3), 779–788. https://doi.org/10.5194/nhess-9-779-2009

Campins, J., Genovés, A., Picornell, M. A., & Jansà, A. (2011). Climatology of Mediterranean cyclones using the era-40 dataset. *International Journal of Climatology*, *31*(11), 1596–1614. https://doi.org/10.1002/joc.2183

Candela, J. (1991). The Gibraltar strait and its role in the dynamics of the Mediterranean sea. *Dynamics of Atmospheres and Oceans*, *15*(3), 267–299. https://doi.org/10.1016/0377-0265(91)90023-9

Cavicchia, L., Von Storch, H., & Gualdi, S. (2013). A long-term climatology of medicanes. *Climate Dynamics*, *43*, 1183, 1195. https://doi.org/10.1007/s00382-013-1893-7

Conte, D., & Lionello, P. (2013). Characteristics of large positive and negative surges in the Mediterranean sea and their attenuation in future climate scenarios. *Global and Planetary Change*, *111*, 159–173. https://doi.org/10.1016/j.gloplacha.2013.09.006

Elkut, A. E., Taha, M. T., Abu Zed, A. B. E., Eid, F. M., & Abdallah, A. M. (2021). Wind-wave hindcast using modified ECMWF era-interim wind field in the Mediterranean sea. *Estuarine, Coastal and Shelf Science*, *252*, 107267. https://doi.org/10.1016/j.ecss.2021.107267

Emanuel, K. (2005). Genesis and maintenance of "Mediterranean hurricanes". *Advances in Geosciences*, *2*, 217, 220. https://doi.org/10.5194/adgeo-2-217-2005

Emanuel, K. (2006). Climate and tropical cyclone activity: A new model downscaling approach. *Journal of Climate*, *19*(19), 4797–4802. https://doi.org/10.1175/JCLI3908.1

Fita, L., Romero, R., Luque, A., Emanuel, K., & Ramis, C. (2007). Analysis of the environments of seven Mediterranean tropical-like storms using an axisymmetric, nonhydrostatic, cloud resolving model. *Natural Hazards and Earth System Sciences*, *7*, 41, 56. https://doi.org/10.5194/nhess-7-41-2007

García Lafuente, J., Álvarez Fanjul, E., Vargas, J. M., & Ratsimandresy, A. W. (2002). Subinertial variability in the flow through the strait of Gibraltar. *Journal of Geophysical Research: Oceans*, *107*(C10), 32–39. https://doi.org/10.1029/2001JC001104

Hersbach, H., Bell, B., Berrisford, P., Hirahara, S., Horányi, A., Muñoz-Sabater, J., et al. (2020). The era5 global reanalysis. *Quarterly Journal of the Royal Meteorological Society*, *146*(730), 1999–2049. https://doi.org/10.1002/qj.3803

Hosking, J. R., & Wallis, J. R. (1987). Parameter and quantile estimation for the generalized pareto distribution. *Technometrics*, *29*(3), 339–349. https://doi.org/10.1080/00401706.1987.10488243

Jansà, A. (1997). A general view about Mediterranean meteorology: Cyclones and hazardous weather. In *INM/WMO International Symposium on cyclones and hazardous weather in the Mediterranean*. Palma de Mallorca.

Jordà, G., Gomis, D., Álvarez Fanjul, E., & Somot, S. (2012). Atmospheric contribution to Mediterranean and nearby Atlantic sea level variability under different climate change scenarios. *Global and Planetary Change*, *80–81*, 198–214. https://doi.org/10.1016/j.gloplacha.2011.10.013

Jourdier, B. (2020). Evaluation of era5, merra-2, cosmo-rea6, newa and arome to simulate wind power production over France. *Advances in Science and Research*, *17*, 63–77. https://doi.org/10.5194/asr-17-63-2020

Kalverla, P. C., Holtslag, A. A. M., Ronda, R. J., & Steeneveld, G.-J. (2020). Quality of wind characteristics in recent wind atlases over the north sea. *Quarterly Journal of the Royal Meteorological Society*, *146*(728), 1498–1515. https://doi.org/10.1002/qj.3748

Kennedy, A. B., Westerink, J. J., Smith, J. M., Hope, M. E., Hartman, M., Taflanidis, A. A., et al. (2012). Tropical cyclone inundation potential on the Hawaiian islands of oahu and kauai. *Ocean Modelling*, *52–53*, 54–68. https://doi.org/10.1016/j.ocemod.2012.04.009

Le Traon, P.-Y., & Gauzelin, P. (1997). Response of the Mediterranean mean sea level to atmospheric pressure forcing. *Journal of Geophysical Research: Oceans*, *102*(C1), 973–984. https://doi.org/10.1029/96JC02777

Marcos, M., Jordà, G., Gomis, D., & Pérez, B. (2011). Changes in storm surges in southern Europe from a regional model under climate change scenarios. *Global and Planetary Change*, *77*(3), 116–128. https://doi.org/10.1016/j.gloplacha.2011.04.002

Marcos, M., Tsimplis, M. N., & Shaw, A. G. P. (2009). Sea level extremes in southern Europe. *Journal of Geophysical Research: Oceans*, *114*, C01007. https://doi.org/10.1029/2008JC004912

Medugorac, I., Mirko, O., Ivica, J., Zoran, P., & Miroslava, P. (2018). Adriatic storm surges and related cross-basin sea-level slope. *Journal of Marine Systems*, *181*, 79–90. https://doi.org/10.1016/j.jmarsys.2018.02.005

Menemenlis, D., Fukumori, I., & Lee, T. (2007). Atlantic to Mediterranean sea level difference driven by winds near Gibraltar strait. *Journal of Physical Oceanography*, *37*, 359, 376. https://doi.org/10.1175/JPO3015.1

Menéndez, M., García-Díez, M., Fita, L., Fernandez, J., Mendez, F., & Gutiérrez, J. (2013). High-resolution sea wind hindcasts over the Mediterranean area. *Climate Dynamics*, *42*, 1857–1872. https://doi.org/10.1007/s00382-013-1912-8

Morales-Márquez, V., Orfila, A., Simarro, G., & Marcos, M. (2020). Extreme waves and climatic patterns of variability in the eastern north Atlantic and Mediterranean basins. *Ocean Science*, *16*(6), 1385–1398. https://doi.org/10.5194/os-16-1385-2020

Muis, S., Apecechea, M. I., Dullaart, J., de Lima Rego, J., Madsen, K. S., Su, J., et al. (2020). A high-resolution global dataset of extreme sea levels, tides, and storm surges, including future projections. *Frontiers in Marine Science*, *7*, 263. https://doi.org/10.3389/fmars.2020.00263

Othmani, A., Bejaoui, C., Elhmaidi, C., Devenon, D., Lotfi, J.-L., & Aleya, L. (2017). High-resolution numerical modelling of the barotropic tides in the Gulf of Gabes, eastern Mediterranean sea (Tunisia). *Journal of African Earth Sciences*, *129*, 224–232. https://doi.org/10.1016/j.jafrearsci.2017.01.007

Patlakas, P., Stathopoulos, C., Tsalis, C., & Kallos, G. (2021). Wind and wave extremes associated with tropical-like cyclones in the Mediterranean basin. *International Journal of Climatology*, *41*(S1), E1623–E1644. https://doi.org/10.1002/joc.6795

Pond, & Pickard. (2013). *Introductory dynamical Oceanography* (2nd ed.). Butterworth-Heinemann.

Roland, A., Zhang, Y., Wang, H., Meng, Y., Teng, Y.-C., Maderich, V., et al. (2012). A fully coupled 3d wave-current interaction model on unstructured grids. *Journal of Geophysical Research*, *117*, C00J33. https://doi.org/10.1029/2012JC007952

Romero, R., & Emanuel, K. (2013). Medicane risk in a changing climate. *Journal of Geophysical Research: Atmospheres*, *118*, 5992–6001. https://doi.org/10.1002/jgrd.50475

Romero, R., & Emanuel, K. (2016). Climate change and hurricane-like extratropical cyclones: Projections for north Atlantic polar lows and medicanes based on cmip5 models. *Journal of Climate*, *30*(1), 279–299. https://doi.org/10.1175/JCLI-D-16-0255.1

Sartini, L., Cassola, F., & Besio, G. (2015). Extreme waves seasonality analysis: An application in the Mediterranean sea. *Journal of Geophysical Research: Oceans*, *120*, 6266–6288. https://doi.org/10.1002/2015JC011061

Soukissian, T., Denaxa, D., Karathanasi, F., Prospathopoulos, A., Sarantakos, K., Iona, S., et al. (2017). Marine renewable energy in the Mediterranean sea: Status and perspectives. *Energies*, *10*, 1512. https://doi.org/10.3390/en10101512

Toomey, T., Sayol, J. M., Marcos, M., Jordà, G., & Campins, J. (2019). A modelling-based assessment of the imprint of storms on wind waves in the western Mediterranean sea. *International Journal of Climatology*, *39*(2), 878–886. https://doi.org/10.1002/joc.5849

Tous, M., & Romero, R. (2013). Meteorological environments associated with medicane development. *International Journal of Climatology*, *33*(1), 1–14. https://doi.org/10.1002/joc.3428

Trigo, I. F., Bigg, G. R., & Davies, T. D. (2002). Climatology of cyclogenesis mechanisms in the Mediterranean. *Monthly Weather Review*, *130*(3), 549–569. https://doi.org/10.1175/15200493(2002)130<0549:COCMIT>2.0.CO;2

Vousdoukas, M., Voukouvalas, E., Annunziato, A., Giardino, A., & Feyen, L. (2016). Projections of extreme storm surge levels along Europe. *Climate Dynamics*, *47*, 3171, 3190. https://doi.org/10.1007/s00382-016-3019-5

Vousdoukas, M. I., Mentaschi, L., Voukouvalas, E., Verlaan, M., & Feyen, L. (2017). Extreme sea levels on the rise along Europe's coasts. *Earth's Future*, *5*, 304–323. https://doi.org/10.1002/2016EF000505

Woodworth, P. L., Hunter, J. R., Marcos, M., Caldwell, P., Menéndez, M., & Haigh, I. (2016). Towards a global higher-frequency sea level dataset. *Geoscience Data Journal*, *3*(2), 50–59. https://doi.org/10.1002/gdj3.42

Zhang, Y., & Baptista, A. (2008). Selfe: A semi-implicit Eulerian-Lagrangian finite-element model for cross-scale ocean circulation. *Ocean Modelling*, *21*, 71–96. https://doi.org/10.1016/j.ocemod.2007.11.005

Zhang, Y. J., Ye, F., Stanev, E. V., & Grashorn, S. (2016). Seamless cross-scale modeling with SCHISM. *Ocean Modelling*, *102*, 64–81. https://doi.org/10.1016/j.ocemod.2016.05.002